Attenuation of Weak Spherical Shock Waves in an Accelerating Flow

Tomoaki Watanabe (渡邉 智昭),[1, a)] Moeki Haneda (羽根田 萌生),[2] Yuki Sugino (杉野 友紀),[1] Koji Nagata (長田 孝二),[1] Kento Inokuma (猪熊 建登),[3] and Akihiro Sasoh (佐宗 章弘)[2]

[1)] *Department of Mechanical Engineering and Science, Kyoto University, Kyoto 615-8530, Japan*

[2)] *Department of Aerospace Engineering, Nagoya University, Nagoya 464-8603, Japan*

[3)] *Institute of Fluid Science, Tohoku University, Sendai 980-8577, Japan*

(Dated: 30 June 2025)

This study reports experimental investigations of a weak spherical shock wave propagating into an accelerating flow induced by a fan. Pressure measurements are conducted for shock waves propagating in both a static fluid and an accelerating flow, and comparisons reveal the influence of the accelerating flow on shock wave properties. The pressure jump of the shock wave is reduced after propagation in the accelerating flow, indicating attenuation of the shock wave. Greater attenuation is observed with increasing longitudinal velocity gradient in the shock propagation direction, corresponding to higher acceleration. When the velocity gradient becomes sufficiently large, the pressure jump is no longer identifiable, implying the disappearance of the shock wave. This attenuation is consistent with the one-dimensional model of a shock wave crossing a surface with an infinitely large velocity gradient, as the experimental conditions approach those of the model with increasing gradient. The attenuation does not affect the fluctuating behavior of the pressure jump. Additionally, the histogram of pressure jumps suggests that attenuation occurs for all shock waves propagating in the accelerating flow. The present experimental results support the shock wave attenuation predicted by the one-dimensional model, offering new insights into shock wave propagation in non-uniform flows.

[a)] Author to whom correspondence should be addressed: watanabe.tomoaki.8x@kyoto-u.ac.jp

I. INTRODUCTION

Shock waves are fundamental phenomena in many problems related to fluid mechanics. In aerospace engineering, they are observed in engine flows and around aircraft during high-speed flight.[1,2] Supersonic transport (SST) aircraft are known to produce noise issues associated with sonic booms.[3] A sonic boom is the explosive noise generated when shock waves produced by an aircraft reach the ground. Such booms pose serious threats to human environments and wildlife, making them a key environmental concern and a major obstacle to the practical deployment of SSTs.[4] When an aircraft travels at supersonic speeds, conical shock waves are formed at its nose. As these shock waves propagate through atmospheric turbulence, their pressure waveforms evolve into the so-called N-wave, characterised by two steep pressure rises. Observations of such waveforms at multiple locations suggest that they are influenced by atmospheric turbulence.[3] These findings, along with other examples of shock waves propagating in turbulent flows, have led to extensive research on the interaction between turbulence and shock waves.

Both experimental and numerical studies have shown that the interaction between shock waves and turbulence leads to significant changes in both.[5] The interaction occurs not only when a shock wave generated externally propagates into a turbulent flow, but also when turbulence itself generates shock waves through turbulent motions. The former scenario is realized in laboratory experiments using shock tubes and high-speed wind tunnels, where shock waves are generated either by diaphragm rupture or by flow over a ramp, respectively. [6–8] It is also reproduced in numerical simulations, where shock waves generated by initial or boundary conditions propagate into turbulence.[9–11] The latter scenario is commonly observed in turbulence with a high turbulent Mach number M_T, which is defined as the ratio between the root-mean-square value of velocity fluctuations and the speed of sound at the mean temperature.[12–18] In statistically steady isotropic turbulence sustained by solenoidal forcing, shock wave generation due to turbulence occurs for $M_T \gtrsim 0.6$[14], although this threshold is not universal and may vary depending on the flow configuration.[19,20] Compression induced by shock waves amplifies velocity fluctuations and reduces the characteristic length scales of turbulence.[21–25] The amplification of velocity gradients, dominated by small-scale turbulent motions, results in deviations from the universal relationship between velocity gradient flatness and the turbulent Reynolds number known for incompressible turbulence.[20] Turbulence

deforms shock waves and induces fluctuations in shock wave properties such as the Mach number.[22,26–28] As turbulence intensity increases, greater deformation occurs, and the shock Mach number, defined as the ratio between the shock propagation velocity and the speed of sound, and related quantities, such as the pressure jump across the shock wave, fluctuate more significantly.[29,30] These pressure jump fluctuations have been shown to correlate with shock wave deformation.[26,31] When a portion of the shock front is ahead of the rest, the surface becomes locally convex when viewed from the front. This convex region tends to have a lower Mach number, resulting from local shock wave attenuation by turbulence. Conversely, a locally concave region, where the wavefront lags behind, exhibits a higher local Mach number. These relationships between shock geometry and Mach number in turbulent flows are consistent with early studies on deformed shock waves.[32,33] Such amplification and attenuation of shock waves have been observed in both experiments and numerical simulations under various shock and turbulence conditions.[6,34–37]

Shock wave deformation in turbulence can originate from the non-uniform velocity of shock propagation, which arises from the inhomogeneous velocity distribution of turbulence.[38] A convex region is typically formed when the shock wave propagates into a region of backward flow relative to the direction of shock propagation, causing a local reduction in shock speed.[31] Similar trends were reported in an early study of a shock wave propagating in a jet issued with or against the shock direction.[39] These studies suggest that the flow direction ahead of the shock wave is a crucial factor in determining the influence of turbulence on shock behaviour. In connection with these experimental and numerical findings, recent theoretical work has examined a Riemann problem, a one-dimensional formulation of a shock wave propagating in a non-uniform flow.[40] The model considers a shock wave propagating from a static fluid into a forward-moving flow and predicts that such propagation results in attenuation of the shock wave. This behaviour aligns with observations of shock–turbulence interaction. The model further suggests that the shock wave may vanish, transitioning into a sound wave depending on the Mach numbers of the shock and the forward flow. It implies that attenuation occurs when the shock experiences acceleration between the static and forward flow regions. However, a critical assumption in the model is that the velocity changes discontinuously across the boundary of the two regions, with the acceleration, defined as the longitudinal velocity gradient in the direction of shock propagation, $\partial U/\partial x$, modelled as a delta function, i.e., $\partial U/\partial x \to \infty$ at the boundary. While the model offers useful insight

for future studies on shock attenuation and control, such a discontinuous velocity jump is difficult to realise in laboratory conditions, and the model predictions have not been experimentally validated. As a more realistic scenario, one can consider a shock wave propagating in an accelerating flow with finite $\partial U/\partial x$. The present study experimentally investigates this case by examining a weak spherical shock wave propagating in an accelerating flow. The results support the theoretical model, confirming that the shock wave is attenuated during propagation in the accelerating flow, with stronger attenuation observed as the acceleration parameter $\partial U/\partial x$ increases.

The above model, which considers a shock wave crossing a surface with an infinitely large velocity gradient, is a one-dimensional problem.[40] In contrast, the interaction between turbulence and shock waves is a more complex, three-dimensional phenomenon. However, a shock wave propagating through such a complex turbulent velocity field locally encounters acceleration that can, in part, be represented by a longitudinal velocity gradient in the direction of shock propagation. Under certain conditions, the local behavior of the shock wave in turbulence can resemble that of a shock wave propagating through a simplified accelerating flow as described by the one-dimensional model. This one-dimensional model has been previously combined with modeled probability distributions of turbulent velocity fluctuations to predict conditions under which local shock disappearance may occur in turbulence.[40] Experiments involving planar shock waves propagating through turbulence have confirmed the occurrence of local shock disappearance under the predicted conditions. A similar approach has also been applied using another simplified model that considers shock wave deformation due to a non-uniform velocity field.[29] In that study, the response of the shock wave to a prescribed tangential velocity distribution was combined with turbulence scaling arguments and a Gaussian-based probability distribution of velocity fluctuations to predict the statistical properties of post-shock pressure fluctuations. The predictions were shown to be consistent with experimental observations of shock waves propagating in turbulence.[29,41,42] Although the one-dimensional model does not capture the full complexity of shock wave behavior in turbulent flows, it serves as a useful and tractable framework. When coupled with statistical representations of turbulence, it provides meaningful insight into the mechanisms of shock/turbulence interaction and broadens the applicability of simplified models to more realistic flow conditions.

The paper is organized as follows. The experimental setup is described in § II. Section III

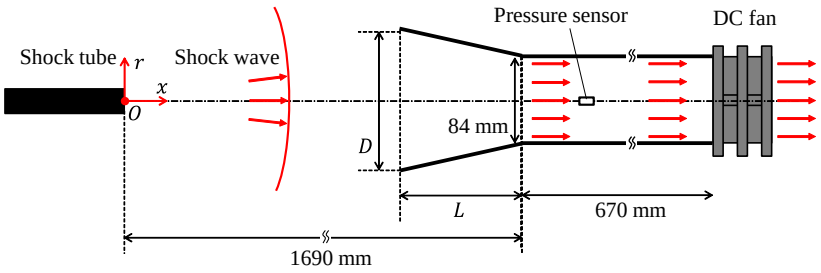

FIG. 1. Experiments of a spherical shock wave propagating into an accelerating flow.

presents the measurement results, detailing the shock wave properties as they propagate in an accelerating flow. Finally, the paper is summarized in § IV.

II. EXPERIMENTS OF A SHOCK WAVE PROPAGATING IN AN ACCELERATING FLOW

Experiments are conducted on a weak spherical shock wave propagating into an accelerating flow. Figure 1 illustrates the experimental setup. The main components are a diaphragmless shock tube system and a DC-fan-operated wind tunnel. A spherical shock wave is emitted from the open end of the shock tube and propagates into the tubular pipe of the wind tunnel, where a fan at the opposite end induces a flow. A pressure sensor is mounted inside the pipe to measure pressure variations caused by the shock wave. The pipe component on the inflow side can be replaced to vary the diameter. The inner diameter at the inflow is denoted by D, and the diameter linearly increases to 84 mm over a length of L. By varying D and L, different velocity profiles can be generated. The flow accelerates from the outside to the inside of the pipe. The open end of the shock tube is defined as the coordinate origin, with x and r denoting the streamwise and radial directions, respectively. The distance from the shock tube end to the throat of the wind tunnel is fixed at 1.69 m. This value is chosen to exclude the early stage of the spherical shock wave propagation (e.g., $x < 1$ m) from the pressure measurements, as the shock Mach number declines rapidly in this region. This setup also allows the distances from the pressure sensor to both the shock tube end and the throat to remain constant when exploring the effects of L and D. Shock

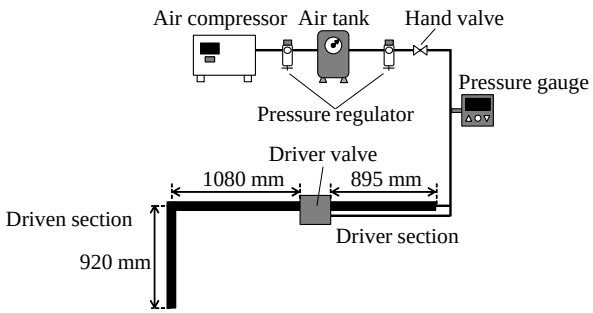

FIG. 2. Schematic of the shock tube system.

wave properties are compared between cases with and without flow. Each experiment is repeated 250 times, and ensemble averages are used to evaluate the shock wave statistics. This section describes the diaphragmless shock tube system, the accelerating flow generator, and the measurement methods.

A. Diaphragmless shock tube and accelerating flow generator

This study employs the diaphragmless shock tube system developed in Ref. 43. A brief overview is provided here, while further details and shock wave characteristics can be found in Ref. 43. Figure 2 shows a schematic of the shock tube system. The shock tube is driven by a valve system composed of multiple air-operated valves. The main valve is actuated by a secondary air-operated sub-valve, which is electrically controlled. Pressurized air from an air tank is supplied to the driver section via a pressure regulator and an air dryer. The driver section consists of a stainless steel pipe, 895 mm in length and 20 mm in inner diameter. When the main valve opens, compressed air flows into the driven section, which is an L-shaped stainless steel pipe with an inner diameter of 20 mm and a total length of 1080 mm + 920 mm, as shown in Fig. 2. The pressure in the driver section is monitored using a digital pressure gauge. The initial driver gas pressure is adjusted by the regulator. Upon valve activation, the compressed air moves from the driver to the driven section, forming a shock wave in the shock tube. This shock wave is ejected from the open end of the driven section and propagates as a spherical shock wave.

All experiments are conducted with an initial driver gas pressure of 900 kPaG, while the

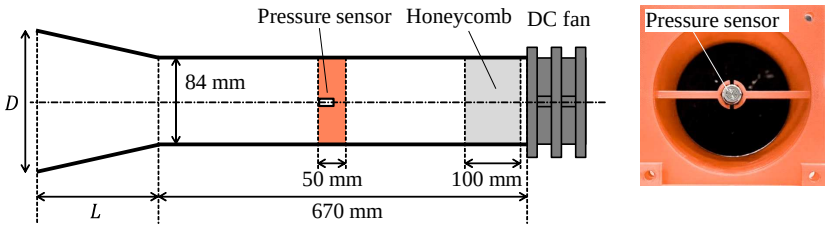

FIG. 3. Schematic of the accelerating flow generator.

driven section is filled with air at atmospheric pressure. Under these conditions, the shock Mach number in the shock tube reaches approximately 1.4, as estimated from pressure measurements.[43] The generated shock wave exhibits minor variations with each operation. The standard deviation of the pressure jump is less than 3% of the mean pressure jump, based on ensemble averages from repeated experiments.[43] Thus, shock waves with consistent characteristics are generated reliably. This level of repeatability is comparable to that achieved by other diaphragmless shock tube systems reported in the literature.[34,44]

Figure 3 shows a schematic of the accelerating flow generator. A DC fan unit consisting of counter-rotating fans (San Ace 92 9CRA0912P0G001) is installed on the outflow side. A honeycomb with a length of 100 mm is placed inside the pipe to remove the swirling component of the flow. The straight pipe, with a total length of 670 mm, is equipped with a pressure sensor (PCB Piezotronics Inc. 113B27), mounted at the center of the pipe as shown in Fig. 3. Comparison with measurements using a sensor mounted on a metallic plate[43] has confirmed that the present sensor setup accurately captures pressure variations caused by the spherical shock wave. The straight pipe is composed of several short segments connected by flanges, allowing the position of the pressure sensor to be adjusted by replacing pipe components. Table I summarizes the sets of D and L used in the experiments. It also includes the mean velocity U in the x direction measured at $x = 1.69$ m, as well as the mean velocity gradient $\partial U/\partial x$. Since $\partial U/\partial x$ varies along the streamwise direction, the maximum values along the pipe centerline are reported in the table. The fan-induced flow velocity varies depending on the conditions, enabling the generation of accelerating flows with different streamwise velocity gradients $\partial U/\partial x$. A smaller D leads to a pressure rise on the suction side of the fan, resulting in a higher velocity.

TABLE I. Experimental conditions.

Case	D (mm)	L (mm)	U (m/s)	$\partial U/\partial x$ (1/s)	u_{rms}/U	Re_λ
1	63	60	20.3	3.4×10^{-1}	0.28%	6.2
2	70	60	17.4	2.9×10^{-1}	0.35%	6.3
3	77	60	14.8	2.2×10^{-1}	0.52%	2.4
4	84	60	13.2	1.9×10^{-1}	0.35%	0.8
5	91	60	11.7	1.6×10^{-1}	0.72%	6.9
6	98	60	11.9	1.5×10^{-1}	0.66%	4.2
7	105	60	10.4	1.2×10^{-1}	0.59%	2.8
8	112	60	10.1	1.1×10^{-1}	0.49%	1.5
9	116	60	9.8	9.8×10^{-2}	0.64%	2.2
10	121	60	9.6	8.8×10^{-2}	0.57%	1.6
11	168	60	9.2	1.1×10^{-1}	0.85%	1.6
12	168	120	9.6	8.1×10^{-2}	0.80%	0.9
13	168	180	9.9	6.7×10^{-2}	1.05%	1.3

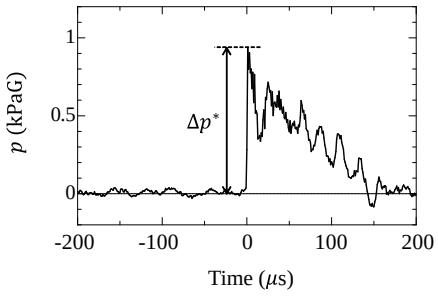

FIG. 4. Pressure variation due to the spherical shock wave measured at $x = 1$ m.

B. Measurement methods

Pressure variations caused by the shock wave are measured using the pressure sensor. The sensor signal is recorded by a digital oscilloscope (YOKOGAWA, DL850E) at a sampling frequency of 1 MHz. The current study also employs an external pressure sensor mounted

on a metallic plate, as described in Ref. 43. This sensor is the same model as the one used inside the pipe and is positioned at approximately the same x location, but outside the pipe. The pressure signal from the external sensor is monitored in each experiment and used to trigger the internal sensor measurements within the relevant time window. Specifically, the oscilloscope records the pressure signals measured before and after the moment of shock wave detection by the external sensor. Figure 4 shows an example of the pressure variation $p(t)$ measured at 1 m from the shock tube exit. A rapid pressure increase occurs upon the arrival of the shock wave, followed by a gradual decrease due to the expansion wave. This waveform is typical of spherical shock waves and is consistent with previous studies.[26,45,46] The pressure jump Δp^* is evaluated as the difference between the peak pressure and the time-averaged pressure, as illustrated in Fig. 4. The time average is taken over 200 μs before the shock wave detection. Due to the reflection of the shock wave at the sensor, the measured pressure jump Δp^* differs from the actual shock-induced pressure jump Δp. For regular reflection of a weak shock wave, Δp can be estimated from Δp^* using the relation $\Delta p = 0.5\Delta p^*(1+\cos\theta)$, where $\theta = \pi/2$ is the angle between the shock normal and the sensor mounting plane.[47] In the present shock tube, the spherical shock wave is considered weak, with a Mach number as low as 1.003. This θ-dependent relation has been validated for spherical shock waves within a Mach number range similar to that in the present experiments.[41]

The mean velocity induced by the fan is measured using a hot-wire anemometer (KANOMAX, Model 6501). The probe is inserted through a small hole on the side of the pipe. Pipe components with different hole positions are used to measure the velocity at various x locations. The measurements are conducted both at the center of the pipe and near the wall. Additional velocity measurements were conducted using a constant-temperature hot-wire anemometry system (StreamLine, Dantec Dynamics) equipped with an I-type probe (55P01, Dantec Dynamics) to assess the characteristics of velocity fluctuations. The sampling size and frequency were set to 8,388,608 and 50kHz, respectively. The probes are inserted into the pipe only during the velocity measurements. Thus, the pressure measurements are free from the influence of the invasive probe.

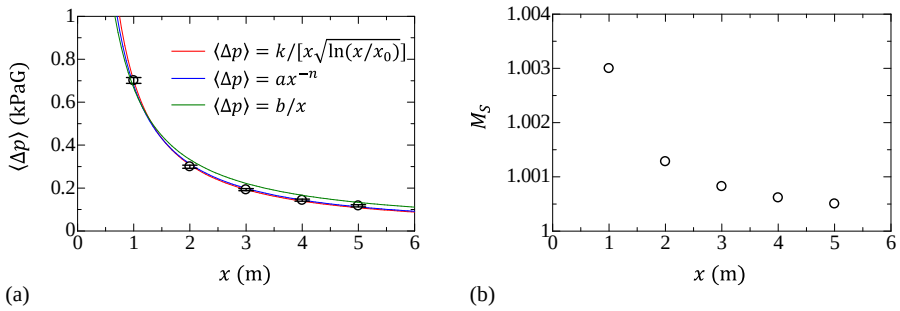

FIG. 5. The decay of (a) mean pressure jump and (b) shock Mach number. The error bars in (a) represent the root-mean-square fluctuations of pressure jump.

III. RESULTS AND DISCUSSION

A. Decay of the spherical shock wave

The properties of the spherical shock wave are examined prior to the experiments involving propagation into an accelerating flow. The pressure waveform of the spherical shock wave is measured using a pressure sensor (PCB Piezotronics Inc. 113B27) incorporated into the pressure measurement system developed in Ref. 43. Measurements are performed at various distances x from the open end of the shock tube: $x = 1, 2, \ldots, 5$ m. At each location, the measurement is repeated 50 times, and the average pressure jump of the shock wave, Δp, is evaluated. Figure 5(a) presents the averaged pressure jump, $\langle \Delta p \rangle$, as a function of x. The decay of a spherical shock wave is known to follow the relation:[48]

$$\langle \Delta p \rangle = \frac{k}{x\sqrt{\ln(x/x_0)}}, \tag{1}$$

where k and x_0 are parameters. The red line in Fig. 5(a) represents Eq. (1) with $k = 1.0834$ kPa·m and $x_0 = 0.0907$ m, obtained via least-squares fitting. Another simple relation is given by a power law[49]:

$$\langle \Delta p \rangle = a x^{-n}. \tag{2}$$

The exponent n varies with the shock Mach number M_S: specifically, n decreases as M_S approaches unity. For a sound wave, $n = 1$ is derived as the asymptotic state of a spherical

shock wave after sufficient decay ($M_S \to 1$).[49] For comparison, Eq. (2) with parameters obtained via least-squares fitting is shown as the blue line. The present results yield $n = 1.12$ and $a = 0.677$ for $\langle \Delta p \rangle$ in kilo pascals (kPa) and x in meters (m). Both Eqs. (1) and (2) show good agreement with the experimental data. Additionally, the green line represents the sound wave case, namely $\langle \Delta p \rangle = bx^{-1}$, where $b = 0.666$ kPaG·m is also determined via least-squares fitting. The observed decay in $\langle \Delta p \rangle$ in the current experiments is faster than x^{-1}. It has been confirmed that a spherical shock wave decays more rapidly than $1/x$,[49] which is consistent with the present measurement results.

The shock Mach number is estimated from the mean pressure jump using the Rankine–Hugoniot relation:

$$\frac{\langle \Delta p \rangle}{p_0} = \frac{2\gamma}{\gamma + 1}(M_S^2 - 1), \tag{3}$$

where p_0 is the ambient pressure and γ is the specific heat ratio. Figure 5(b) shows the variation of M_S with distance. The shock wave has a shock Mach number of 1.4 in the shock tube. Once the shock wave is emitted from the shock tube, it spherically expands, significantly reducing the shock Mach number. The shock Mach number decreases to as low as 1.0005. Other shock tube facilities have also observed this rapid decay.[34] The experiments involving shock wave propagation into an accelerating flow are conducted for $x > 1$ m, where the shock Mach number is below 1.003. Specifically, most pressure measurements are conducted at $x = 2.000$ m for a weak spherical shock wave with a pressure jump on the order of 300 Pa, corresponding to a shock Mach number $M_S \approx 1.0015$. The focus of this study is to investigate the behavior of such weak shock waves propagating in an accelerating flow. Although it is of interest to explore the influence of the shock Mach number, several limitations inherent to the experimental setup prevent a systematic parametric study. Previous experimental and numerical studies have shown that shock wave modulation due to non-uniform flows is governed by the parameters $M_S - 1$ and $M_S^2 - 1$, which must vary over several decades (e.g., from 10^{-4} to 10^{-1}) to reveal meaningful Mach number dependence.[21,22,29,30,50] However, the spherical shock wave exhibits a power-law decay with distance, and at positions beyond $x = 2$ m, the Mach number varies only slightly. Therefore, simply extending the measurement distance does not provide sufficient variation in M_S for investigating its influence. Based on our prior measurements near the shock tube exit without the accelerating flow facility,[43] investigations into M_S dependence require sensor placement within $x < 0.5$

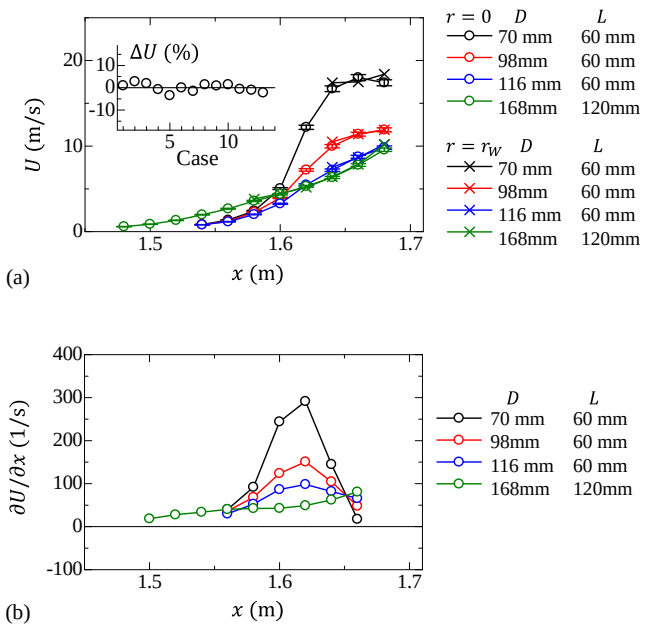

FIG. 6. (a) Mean velocity variations in the x direction along the centerline ($r = 0$) and near the wall ($r = r_W$). The error bars indicate possible measurement errors due to the current hot-wire anemometry system, which are 2% of the mean velocity. The inset shows the velocity difference between the center and the near-wall region, defined as $\Delta U = (U_{r=0} - U_{r=r_W})/U_{r=0}$ for all cases. (b) Mean velocity gradient $\partial U/\partial x$.

m. However, this region is not accessible in the current setup due to mechanical and aerodynamic interference between the shock tube and the accelerating flow generator. For these reasons, the present study is limited to a weak shock wave, and the primary focus is placed on the systematic variation of the acceleration parameter $\partial U/\partial x$, which is shown to strongly influence the shock wave propagation.

B. Flow properties

The accelerating flow induced by the fan is characterized by velocity measurements. Figure 6(a) presents the mean velocity profiles for four representative (L, D) cases. Similar

trends have been observed under other conditions. Measurements are taken along the centerline at $r = 0$, and additional measurements are performed near the wall at $r = r_W$, located 15 mm from the wall. From the inlet, the mean velocity increases with x, indicating the formation of accelerating flows with $\partial U/\partial x > 0$. The mean velocity values are similar between the center and near-wall regions. The inset in Fig. 6(a) shows the relative velocity difference ΔU between these regions for all (L, D) sets. In all cases, the difference is less than 5%. Although the diameter change from the inlet could potentially cause flow separation, forming a highly inhomogeneous flow, such effects are negligible at 15 mm from the wall in the present experiments. As a result, the flow near the center remains approximately uniform across the inlet region through which the shock wave propagates.

Figure 6(b) shows the mean velocity gradient $\partial U/\partial x$. The value of $\partial U/\partial x$ varies depending on the combination of (L, D). For other conditions, the corresponding $\partial U/\partial x$ values are presented later along with the shock wave measurement results. In general, a smaller diameter leads to a larger velocity gradient. It is also observed that a smaller L increases $\partial U/\partial x$, although the gradient is more sensitive to changes in D than in L.

A time-series of instantaneous velocity, $\tilde{u}(t)$, measured at a fixed location using the I-type probe of the hot-wire anemometry system, is decomposed into the time-averaged velocity U and the fluctuating component u. The time average of a quantity f is denoted by $\overline{f}$. The root-mean-square (rms) of the velocity fluctuations is defined as $u_{rms} = \sqrt{\overline{u^2}}$. The turbulent Reynolds number is given by $Re_\lambda = u_{rms}\lambda/\nu$, where ν is the kinematic viscosity and $\lambda = u_{rms}/\sqrt{\overline{(\partial u/\partial x)^2}}$ is the Taylor microscale. The velocity gradient $\partial u/\partial x$ is estimated using Taylor's frozen turbulence hypothesis as $\partial u/\partial x = -(1/U)(\partial u/\partial t)$. Table I presents the turbulence intensity u_{rms}/U and Re_λ measured at the entrance of the wind tunnel. The rms velocity fluctuations are found to be less than 1%, and the turbulent Reynolds number remains below 10. These results indicate that the inflow to the wind tunnel is laminar and that the velocity fluctuations are unlikely to influence the shock propagation.

C. Shock wave propagation in the accelerating flow

The effect of propagation through an accelerating flow on the shock wave is investigated using pressure measurements. Figure 7 presents the variation of the mean pressure jump $\langle \Delta p \rangle$ as a function of x, obtained from experiments conducted with different pressure sensor

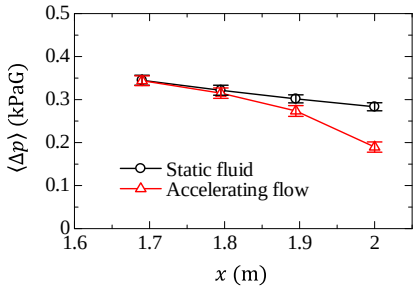

FIG. 7. Variations in the mean pressure jump of the shock wave propagating in a static fluid or accelerating flow, The experiments are conducted with $(D, L) = (84\text{ mm}, 60\text{ mm})$.

locations within the straight pipe. When the fan is turned off, the shock wave propagates through a static fluid in the pipe. Due to the natural decay of a spherical shock wave, $\langle \Delta p \rangle$ decreases slightly with x, consistent with the decay observed in free space, as shown in Fig. 3. When the shock wave propagates through the accelerating flow, $\langle \Delta p \rangle$ becomes smaller than in the baseline static-fluid case. This reduction in pressure jump is consistent with the one-dimensional model,[40] which attributes the decrease to the propagation of expansion waves. Here, the model assumes that a shock wave propagates into a surface of infinitely large acceleration (i.e., $\partial U/\partial x \to \infty$). In contrast, the acceleration field in the present experiments is spatially distributed and finite. Therefore, a direct quantitative comparison with the experimental results is not feasible. Nonetheless, the experimental results qualitatively agree with the model prediction: the shock wave is attenuated as it propagates through the accelerating flow. The present results show that the reduction in $\langle \Delta p \rangle$ becomes more pronounced with increasing x, indicating that the pressure jump decreases progressively as the shock wave travels through the accelerating flow. This behavior is consistent with findings from DNS and experiments on shock waves in turbulent flows, where the effects of turbulence on the shock wave emerge after a certain propagation distance.[30,38,40]

The error bars in Fig. 7 represent the root-mean-square (rms) fluctuations of Δp over 250 experiments, defined as $\Delta p_{rms} = \sqrt{\langle \Delta p^2 \rangle - \langle \Delta p \rangle^2}$. Even when the shock wave propagates in a static fluid, slight variations occur between experiments, and $\Delta p_{rms} \approx 0.02$ kPaG, which is about 6% of the mean pressure jump. This variability is attributed to the characteristics of the shock tube system.[43] It is known that Δp_{rms} increases when shock waves interact with

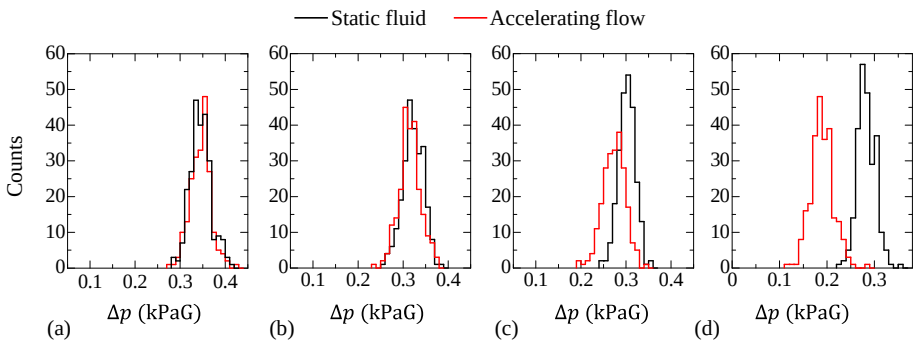

FIG. 8. Histograms of the pressure jump of the shock wave measured at (a) $x = 1.690$ m, (b) $x = 1.795$ m, (c) $x = 1.895$ m, and (d) $x = 2.000$ m. The experiments are conducted with $(D, L) = (84\text{ mm}, 60\text{ mm})$.

turbulence. However, in the present experiments, even with propagation in an accelerating flow, $\Delta p_{rms} \approx 0.02$ kPaG remains nearly unchanged, suggesting that the interaction within the accelerating flow does not significantly enhance fluctuations in the pressure jump.

Figure 8 presents the histograms of Δp measured at four positions along the x direction. At $x = 1.69$ m, the distribution of Δp is nearly identical between the static fluid and the accelerating flow cases. As the shock wave propagates further in the x direction, the distribution shifts toward smaller Δp values without a significant change in shape. By $x = 2.00$ m, almost all shock waves propagating in the accelerating flow exhibit smaller Δp than those in the baseline static fluid case, indicating that attenuation occurs in all experiments.

The dependence on the velocity distribution is examined by comparing Δp statistics across different (D, L) configurations, with pressure measurements conducted at $x = 2.000$ m. Figure 9 shows the mean pressure jump $\langle \Delta p \rangle$ as a function of either D or L. When a shock wave propagates through a pipe with varying diameter, it tends to weaken in an expanding section and strengthen in a contracting one.[51] This geometric effect causes a slight reduction in $\langle \Delta p \rangle$ for smaller D. However, the influence of the accelerating flow is substantially greater than this geometric effect. As D decreases, $\langle \Delta p \rangle$ drops rapidly. Variations in L with $D = 168$ mm have little to no effect on $\langle \Delta p \rangle$ for shock waves propagating in the accelerating flow. Figure 9(a) does not include the plot for $D = 63$ mm, as no distinct pres-

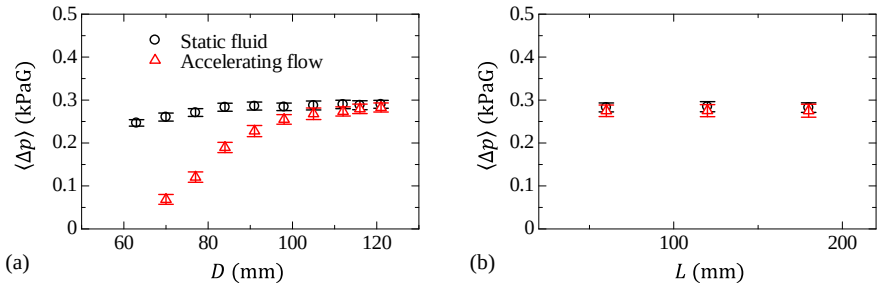

FIG. 9. The mean pressure jumps $\langle \Delta p \rangle$ of the shock wave propagating in a static fluid or accelerating flow: (a) D dependence with $L = 60$ mm; (b) L dependence with $D = 168$ mm. The measurements are conducted at $x = 2.000$ m.

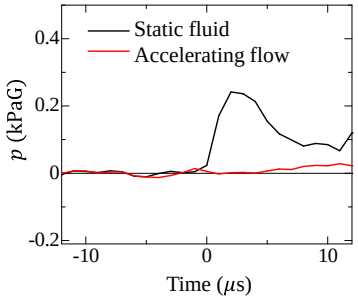

FIG. 10. Pressure variation of the shock wave propagating in an accelerating flow or a static fluid for the case of $D = 63$ mm and $L = 60$ mm. Measurements are conducted at $x = 2.000$ m.

sure jump was identified, suggesting that the shock wave likely vanished. Figure 10 presents examples of instantaneous pressure variations for the case of $D = 63$ mm and $L = 60$ mm. In this plot, time $t = 0$ corresponds to the shock wave detection time in the static fluid case. No such pressure jump is observed in the accelerating flow case with $D = 63$ mm, indicating that the shock wave has disappeared.

Although the velocity gradient $\partial U/\partial x$ vanishes beyond $x \approx 1.65$ m, as shown in Fig. 6, the influence of the upstream accelerating region persists and affects the shock wave behavior even at $x = 2$ m. This is due to the non-local and non-stationary nature of shock wave interactions with non-uniform flows. Previous experimental and numerical studies on

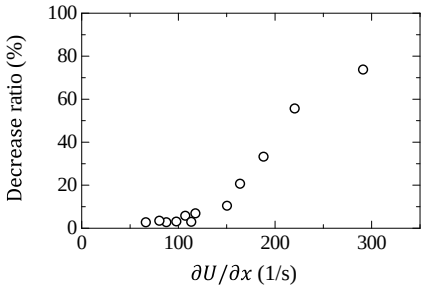

FIG. 11. The decrease ratio in $\langle \Delta p \rangle$ by the propagation in the accelerating flow, plotted as a function of the maximum velocity gradient $\partial U/\partial x$. The measurements are conducted at $x = 2.000$ m.

shock waves interacting with turbulence or individual vortices have shown that the effects of flow inhomogeneities (e.g., velocity fluctuations in turbulence) are not confined to their spatial location. Instead, the shock response, such as fluctuations in shock Mach number or pressure jump, emerges with a time delay and continues even after the shock exits the disturbed region.[29,31,38,52,53] These phenomena have been confirmed via spatiotemporal correlations between pre-shock flow structures and post-shock pressure fluctuations. Similar behavior is also observed when a shock wave exits turbulence and enters a laminar region. Even after entering the laminar flow, significant shock Mach number fluctuations persist, indicating continued influence from the past turbulent field.[41,42] These findings suggest that the acceleration field at $x \lesssim 1.6$ m modifies the shock wave, leading to measurable effects at $x = 2$ m.

The above results are summarized by plotting the reduction ratio of $\langle \Delta p \rangle$ from the baseline case as a function of the velocity gradient $\partial U/\partial x$ in Fig. 11. The velocity gradient is evaluated at the location where $\partial U/\partial x$ reaches its maximum. The decrease in pressure jump is strongly correlated with the velocity gradient, which characterizes the streamwise acceleration. In the present experiments, significant attenuation of the shock wave occurs once $\partial U/\partial x$ exceeds approximately 150 s^{-1}. In the one-dimensional model of a shock wave propagating into a forward flow from a static fluid, the pressure jump is reduced due to expansion waves.[40] The model predicts that the shock wave disappears when the following

condition is met:

$$M = \frac{U}{a} \geq \frac{4}{\gamma + 1} \frac{M_S^2 - 1}{M_S}, \tag{4}$$

where M is the Mach number and a is the speed of sound in the forward flow region. At the pressure measurement location with $M_S \approx 1.0015$, Eq. (4) yields a threshold velocity of $U \gtrsim 1.7$ m/s. In the experiments, the mean velocity induced by the fan exceeds 9 m/s, satisfying this criterion. Nevertheless, a clear pressure jump due to the shock wave is observed in most cases except for case 1. As discussed in the introduction, the key difference between the model and the experiments lies in the assumption of a discontinuous velocity field in the model. In the model, the shock wave propagates across an infinitely thin interface separating the static and forward flow regions, resulting in $\partial U/\partial x \to \infty$. In contrast, the experiments involve a gradual acceleration with finite $\partial U/\partial x$, as the shock wave propagates through a continuously varying velocity field. This difference explains the weaker effect of the forward flow on the shock wave in the experimental results. However, as $\partial U/\partial x$ increases, the experimental conditions approach those of the model. Indeed, the present experiments confirm that the attenuation effect becomes more pronounced with increasing $\partial U/\partial x$, and in case 1, the shock wave is no longer detectable in the pressure measurements when $\partial U/\partial x$ exceeds 300 s^{-1}. These results are qualitatively consistent with the one-dimensional model proposed in Ref. 40.

In the present experimental setup, shock attenuation due to the accelerating flow becomes prominent for $\partial U/\partial x > 150$ s^{-1}, and the shock wave disappears when $\partial U/\partial x > 300$ s^{-1}. These thresholds should not be considered universal. Due to limitations of the shock tube system and the inherent decay of the spherical shock wave, the current investigation is restricted to a single, low shock Mach number condition. Clarifying the conditions under which shock wave attenuation becomes significant requires further parametric studies on the shock Mach number M_S, which are beyond the scope of the present work.

Figure 12 compares the histogram of the pressure jump between shock waves propagating in a static fluid and those in an accelerating flow for four different D cases. A decrease in D, which results in a larger $\partial U/\partial x$, leads to a reduction in the mean pressure jump, as shown in Figs. 9 and 11. In the accelerating flow cases, the histogram of Δp shifts toward smaller values compared to the baseline static-fluid cases, with this shift becoming more pronounced as D decreases. This change in the histogram indicates that shock wave attenuation due to

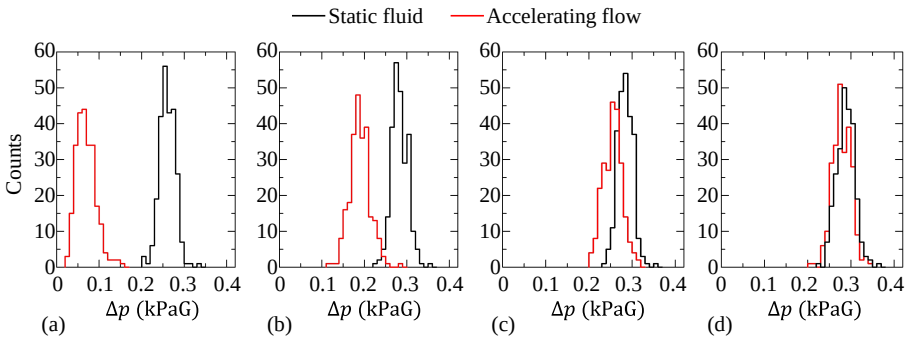

FIG. 12. Histograms of the pressure increase of the shock wave measured with (a) $D = 70$ mm, (b) $D = 84$ mm, (c) $D = 98$ mm, and (d) $D = 116$ mm. All experiments are conducted with $L = 60$ mm. The measurements are conducted at $x = 2.000$ m.

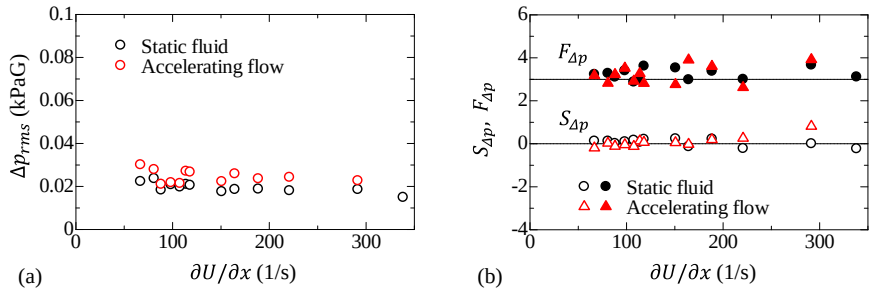

FIG. 13. (a) Rms fluctuations Δp_{rms} of pressure jump. (b) Skewness $S_{\Delta p}$ and flatness $F_{\Delta p}$ of pressure jump. The horizontal lines in (b) represent the skewness and flatness values for Gaussian probability distributions. The measurements are conducted at $x = 2.000$ m.

the accelerating flow consistently occurred in every experiment.

Figure 13 shows the statistical properties of pressure jump fluctuations, defined as $\Delta p' = \Delta p - \langle \Delta p \rangle$. The root-mean-square (rms) fluctuations, $\Delta p_{rms} = \sqrt{\langle \Delta p'^2 \rangle}$, are presented in Fig. 13(a) as functions of the velocity gradient for the accelerating flow cases. Interaction with the accelerating flow slightly increases Δp_{rms}. It is known that velocity fluctuations in front of the shock wave induce fluctuations in the pressure jump. However, the increase in Δp_{rms} is similar across different (D, L) configurations, despite varying levels of shock wave

attenuation.

IV. CONCLUSION

Experiments have been conducted on a weak spherical shock wave propagating into an accelerating flow induced by a fan, with the aim of reproducing the shock attenuation due to forward flow as predicted by a one-dimensional model.[40] The present experiments confirm that the pressure jump of the shock wave decreases after propagation through the accelerating flow. This attenuation becomes more pronounced as the shock wave encounters stronger acceleration, characterized by a larger longitudinal velocity gradient $\partial U/\partial x$. The shock attenuation effect predicted by the model is based on a shock wave propagating toward a surface with an infinitely large velocity gradient, $\partial U/\partial x \to \infty$. The observed dependence on $\partial U/\partial x$ in the present study is consistent with this model, as the experimental conditions increasingly resemble the idealized scenario at higher velocity gradients. Furthermore, in cases with very large $\partial U/\partial x$, the pressure jump of the shock wave could not be identified, suggesting the disappearance of the shock wave. This is also in agreement with the model, which also predicts that the shock wave is eliminated by propagating into a forward flow region. The spherical shock wave exhibits small fluctuations in pressure jump. These fluctuations are largely unaffected by the attenuation: the skewness and flatness remain close to 0 and 3, respectively, consistent with a Gaussian probability distribution. Multiple measurements for each experimental condition show that the attenuation effect is consistently observed. Histogram analysis confirms that the shock wave is weakened in every experiment involving accelerating flow.

These results provide experimental support for the shock wave attenuation predicted by the one-dimensional model and offer novel insights into shock wave propagation in non-uniform flows. However, the current investigation is limited to weak shock waves with low Mach numbers due to constraints of the shock tube system. Further experimental and numerical studies are required to fully understand shock wave attenuation in accelerating flows, including quantifying the threshold of the acceleration parameter $\partial U/\partial x$ for attenuation and determining the conditions under which the shock wave disappears.

ACKNOWLEDGMENTS

The authors acknowledge Mr. R. Kato (Nagoya University) for his assistance with the experiments. This work was supported by JSPS KAKENHI Grants JP18J21758 and JP21H04589.

DATA AVAILABILITY

The data that support the findings of this study are available from the corresponding author upon reasonable request.

REFERENCES

[1]G. M. Lilley and A. H. Yates, "Some aspects of noise from supersonic aircraft," J. Roy. Aero. Soc. **57**, 396 (1953).

[2]A. Kawasaki, T. Inakawa, J. Kasahara, K. Goto, K. Matsuoka, A. Matsuo, and I. Funaki, "Critical condition of inner cylinder radius for sustaining rotating detonation waves in rotating detonation engine thruster," Proc. Combust. Inst. **37**, 3461 (2019).

[3]D. J. Maglieri, "Some effects of airplane operations and the atmosphere on sonic-boom signatures," J. Acoust. Soc. Am. **39**, S36 (1966).

[4]C. Cerri, "The effects of sonic boom on the ecological environment," J. Navig. **33**, 296 (1980).

[5]A. Cuadra, M. Di R., J.-J. O. E. Hoste, C. T. Williams, M. Vera, and C. Huete, "Review of shock-turbulence interaction with a focus on hypersonic flow," Phys. Fluids **37**, 045129 (2025).

[6]T. Tamba, G. Fukushima, M. Kayumi, A. Iwakawa, and A. Sasoh, "Experimental investigation of the interaction of a weak planar shock with grid turbulence in a counter-driver shock tube," Phys. Rev. Fluid **4**, 073401 (2019).

[7]T. Guo, J. Zhang, F. Tong, and X. Li, "Amplification of turbulent kinetic energy and temperature fluctuation in a hypersonic turbulent boundary layer over a compression ramp," Phys. Fluids **35**, 046118 (2023).

[8]T. Gan and Q. Wang, "Experimental investigation of unsteady nature of shock waves induced by various ramps," Phys. Fluids **36**, 125106 (2024).

[9]V. K. Veera and K. Sinha, "Modeling the effect of upstream temperature fluctuations on shock/homogeneous turbulence interaction," Phys. Fluids **21** (2009).

[10]C. H. Chen and D. A. Donzis, "Amplification of transverse Reynolds stresses in shock–turbulence interactions," AIAA J. **60**, 6235 (2022).

[11]P. Thakare, V. Nair, and K. Sinha, "Nonlinear scaling of fluctuation kinetic energy for shock–vorticity wave interaction," Phys. Fluids **36**, 056106 (2024).

[12]R. Jahanbakhshi, N. S. Vaghefi, and C. K. Madnia, "Baroclinic vorticity generation near the turbulent/non-turbulent interface in a compressible shear layer," Phys. Fluids **27**, 105105 (2015).

[13]R. Nagata, T. Watanabe, and K. Nagata, "Turbulent/non-turbulent interfaces in temporally evolving compressible planar jets," Phys. Fluids **30**, 105109 (2018).

[14]T. Watanabe, K. Tanaka, and K. Nagata, "Solenoidal linear forcing for compressible, statistically steady, homogeneous isotropic turbulence with reduced turbulent mach number oscillation," Phys. Fluids **33**, 095108 (2021).

[15]Q. Dai, K. Luo, J. Fan, Z. Guo, and Z. Chen, "Fluctuations of thermodynamic variables in compressible isotropic turbulence laden with inertial particles," Phys. Fluids **33**, 093312 (2021).

[16]Q. Dai, X. Zhang, X. Yuan, and W. Feng, "Direct numerical simulation of turbulent structures and asymmetric properties in the supersonic non-isothermal mixing layer," Phys. Fluids **34**, 125118 (2022).

[17]Y. Sakurai and T. Ishihara, "Direct numerical simulations of compressible turbulence in a periodic box: Effect of isothermal assumptions on turbulence statistics," Phys. Fluids **36**, 085152 (2024).

[18]T. Watanabe, T. Inagaki, T. Mori, K. Ishizawa, and K. Nagata, "Direct numerical simulations of the interaction of temporally evolving circular jets," J. Fluid Mech. **1009**, A68 (2025).

[19]R. Jahanbakhshi and C. K. Madnia, "Entrainment in a compressible turbulent shear layer," J. Fluid Mech. **797**, 564 (2016).

[20]K. Yamamoto, T. Ishida, T. Watanabe, and K. Nagata, "Experimental and numerical investigation of compressibility effects on velocity derivative flatness in turbulence," Physics of Fluids **34**, 055101 (2022).

[21]S. Lee, S. K. Lele, and P. Moin, "Direct numerical simulation of isotropic turbulence interacting with a weak shock wave," J. Fluid Mech. **251**, 533 (1993).

[22]J. Larsson, I. Bermejo-Moreno, and S. K. Lele, "Reynolds- and Mach-number effects in canonical shock-turbulence interaction," J. Fluid Mech. **717**, 293 (2013).

[23]J. Keller and W. Merzkirch, "Interaction of a normal shock wave with a compressible turbulent flow," Exp. Fluids **8**, 241 (1990).

[24]K. Sinha, K. Mahesh, and G. V. Candler, "Modeling shock unsteadiness in shock/turbulence interaction," Phys. Fluids **15**, 2290 (2003).

[25]J. H. Agui, G. Briassulis, and Y. Andreopoulos, "Studies of interactions of a propagating shock wave with decaying grid turbulence: velocity and vorticity fields," J. Fluid Mech. **524**, 143 (2005).

[26]J. Kim, A. Sasoh, and A. Matsuda, "Modulations of a weak shock wave through a turbulent slit jet," Shock Waves **20**, 339 (2010).

[27]D. A. Donzis, "Shock structure in shock-turbulence interactions," Phys. Fluids **24**, 126101 (2012).

[28]G. Fukushima, S. Ogawa, J. Wei, Y. Nakamura, and A. Sasoh, "Impacts of grid turbulence on the side projection of planar shock waves," Shock Waves **31**, 101 (2021).

[29]K. Inokuma, T. Watanabe, K. Nagata, and Y. Sakai, "Statistics of overpressure fluctuations behind a weak shock wave interacting with turbulence," Phys. Fluids **31**, 085119 (2019).

[30]K. Tanaka, T. Watanabe, and K. Nagata, "Statistical analysis of deformation of a shock wave propagating in a local turbulent region," Phys. Fluids **32**, 096107 (2020).

[31]K. Tanaka, T. Watanabe, K. Nagata, A. Sasoh, Y. Sakai, and T. Hayase, "Amplification and attenuation of shock wave strength caused by homogeneous isotropic turbulence," Phys. Fluids **30**, 035105 (2018).

[32]G. B. Whitham, "A new approach to problems of shock dynamics Part 1 Two-dimensional problems," J. Fluid Mech. **2**, 145 (1957).

[33]A. D. Pierce, "Statistical theory of atmospheric turbulence effects on sonic-boom rise times," J. Acoust. Soc. Am. **49**, 906 (1971).

[34]A. Sasoh, T. Harasaki, T. Kitamura, D. Takagi, S. Ito, A. Matsuda, K. Nagata, and Y. Sakai, "Statistical behavior of post-shock overpressure past grid turbulence," Shock Waves **24**, 489 (2014).

[35]C. H. Chen and D. A. Donzis, "Shock–turbulence interactions at high turbulence intensities," J. Fluid Mech. **870**, 813 (2019).

[36]K. Inokuma, T. Watanabe, K. Nagata, and Y. Sakai, "Statistical properties of spherical shock waves propagating through grid turbulence, turbulent cylinder wake, and laminar flow," Phys. Scr. , 044004 (2019).

[37]A. Kusuhata, K. Tanaka, T. Watanabe, K. Nagata, and A. Sasoh, "Local geometry of a weak normal shock wave interacting with turbulence," Phys. Fluids **35**, 086110 (2023).

[38]K. Inokuma, T. Watanabe, K. Nagata, A. Sasoh, and Y. Sakai, "Finite response time of shock wave modulation by turbulence," Phys. Fluids **29**, 051701 (2017).

[39]H. S. Ribner, P. J. Morris, and W. H. Chu, "Laboratory simulation of development of superbooms by atmospheric turbulence," J. Acoust. Soc. Am. **53**, 926 (1973).

[40]G. Fukushima, J. Wei, S. Ogawa, J. Hagiwara, Y. Nakamura, and A. Sasoh, "Losing the shock wave front profile due to interaction with turbulence," Fluid Dyn. Res. **53**, 025504 (2021).

[41]K. Aruga, K. Inokuma, T. Watanabe, K. Nagata, and Y. Sakai, "Experimental investigation of interactions between turbulent cylinder wake and spherical shock wave," Phys. Fluids **32**, 016101 (2020).

[42]K. Inokuma, T. Watanabe, K. Nagata, and Y. Sakai, "Experimental study of shock wave modulation caused by velocity and temperature fluctuations in cylinder wakes," Phys. Rev. Fluids **6**, 063401 (2021).

[43]K. Inokuma, T. Maeda, T. Watanabe, and K. Nagata, "Diaphragmless shock tube with multiple air-operated valves," Exp. Fluids **63**, 121 (2022).

[44]S. H. R. Hosseini and K. Takayama, "Experimental study of toroidal shock wave focusing in a compact vertical annular diaphragmless shock tube," Shock Waves **20**, 1 (2010).

[45]B. Lipkens and D. T. Blackstock, "Model experiment to study sonic boom propagation through turbulence. Part I: General results," J. Acoust. Soc. Am. **103**, 148 (1998).

[46]K. Tanaka, T. Watanabe, H. Suzuki, and T. Kouchi, "Spherical shock wave modulation induced by interaction with homogeneous isotropic turbulence," Phys. Fluids **37**, 026114 (2025).

[47]L. Schwer, "Air blast reflection ratios and angle of incidence," in *Proceedings of the 11th European LS-DYNA Conference* (2017) pp. 9–11.

[48]L. D. Landau, "On shock waves at large distances from the place of their origin," J. Phys. USSR **9**, 496 (1945).

[49]C. E. Needham, *Blast waves*, Vol. 402 (Springer, 2010).

[50]J. Larsson and S. K. Lele, "Direct numerical simulation of canonical shock/turbulence interaction," Phys. Fluids **21**, 126101 (2009).

[51]G. Whitham, "On the propagation of shock waves through regions of non-uniform area or flow," J. Fluid Mech. **4**, 337 (1958).

[52]S. Singh, A. Karchani, and R. S. Myong, "Non-equilibrium effects of diatomic and polyatomic gases on the shock-vortex interaction based on the second-order constitutive model of the Boltzmann-Curtiss equation," Phys. Fluids **30**, 016109 (2018).

[53]Y. Lv and Q. Li, "Numerical simulation of shock-microscale vortex interaction," Comput. Fluids **279**, 106308 (2024).